Bubbling route to strange nonchaotic attractor in a nonlinear series *LCR* circuit with a nonsinusoidal force

D. V. Senthilkumar,[1,*] K. Srinivasan,[2] K. Thamilmaran,[1] and M. Lakshmanan[1,†]
[1]*Centre for Nonlinear Dynamics, Department of Physics, Bharathidasan University, Tiruchirapalli 620 024, India*
[2]*Department of Physics, National Institute of Technology, Tiruchirappalli 620 015, India*
(Received 9 April 2008; published 16 December 2008)

We identify an unconventional route to the creation of a strange nonchaotic attractor (SNA) in a quasiperiodically forced electronic circuit with a nonsinusoidal (square wave) force as one of the quasiperiodic forces through numerical and experimental studies. We find that bubbles appear in the strands of the quasiperiodic attractor due to the instability induced by the additional square-wave-type force. The bubbles then enlarge and get increasingly wrinkled as a function of the control parameter. Finally, the bubbles get extremely wrinkled (while the remaining parts of the strands of the torus remain largely unaffected) resulting in the creation of the SNA; we term this the bubbling route to the SNA. We characterize and confirm this creation from both experimental and numerical data using maximal Lyapunov exponents and their variance, Poincaré maps, Fourier amplitude spectra, and spectral distribution functions. We also strongly confirm the creation of a SNA via the bubbling route by the distribution of the finite-time Lyapunov exponents.

DOI: 10.1103/PhysRevE.78.066211 PACS number(s): 05.45.Pq, 05.45.Ac, 05.45.Df

I. INTRODUCTION

Strange nonchaotic attractors (SNAs) are considered as typical structures of quasiperiodically forced nonlinear systems. They are geometrically strange (that is, they are fractal in nature) just like the chaotic attractors, while all their Lyapunov exponents are either zero or negative, which ensures that the underlying dynamics is nonchaotic. Further, due to their fractal nature, the SNAs are characterized by aperiodic oscillations. Following the pioneering work of Grebogi *et al.* [1], SNAs have been extensively investigated theoretically in several dynamical systems [2–20]. The existence of SNAs has also been demonstrated experimentally [21–24] in a few physically relevant situations. As a consequence, several routes (scenarios having distinct signatures) to SNAs have been reported theoretically. These include the Heagy-Hammel route [16], the gradual fractalization route [13], various types of intermittency routes [10,15,19,22], the blowout bifurcation route [6], etc. As all these bifurcation scenarios (routes to SNAs) have been well established in the literature, we summarize the different scenarios for the formation of SNAs along with their distinct signatures and mechanisms in Table I. Reviews on SNAs can be found in Refs. [7,25,26].

As mentioned above, while extensive numerical studies on the creation of SNAs via different routes are available in the literature [2–20], only a few experimental realizations of them exist [21–24]. In particular, these exotic attractors were confirmed by an experiment consisting of a quasiperiodically forced, buckled, magnetoelastic ribbon [23]. SNAs were also realized in analog simulations of a multistable potential [27], and in a neon glow discharge experiment [28]. These attractors were also shown to be related to the Anderson localization phenomenon in the Schrödinger equation with a quasiperiodic potential [17,29]. Very recently, SNAs have also been observed in an excitable chemical system, namely, a three-electrode electrochemical cell [30]. In this connection, from an experimental point of view, nonlinear electronic circuits with suitable quasiperiodic forces turn out to be especially useful dynamical systems for the identification and study of SNAs. For example, the type-I intermittency route to SNA was reported in a quasiperiodically forced Murali-Lakshmanan-Chua circuit [22]. Recently, three prominent routes, namely, Heagy-Hammel, fractalization, and type-III intermittency routes to SNAs, have been identified and reported in a quasiperiodically forced negative conductance series *LCR* circuit with a diode [24] both experimentally and numerically by some of the present authors.

In almost all the above studies, as a general rule, the driving forces are assumed to be sinusoidal in nature. Naturally the question arises as to what happens to the dynamics when one or both of the driving forces are nonsinusoidal but periodic. Can new routes to the creation of SNAs emerge in such a scenario? In order to answer these questions, we consider a quasiperiodically driven negative conductance series *LCR* circuit with a diode (which was investigated in [24]) and unravel the dynamics of the circuit with one of the forces taken as a square wave force (nonsinusoidal) for suitable parameter values. The main reason for choosing the square wave as one of the driving forces is its bistable nature. Bistability is responsible for hysteresis in many physical and technical systems [31–34]. Further, the square wave has also been used for inducing chaos in certain dynamical systems [35]. For example a 10 MHz square wave optical message was injected into a ring laser to produce high-dimensional chaotic light [36]. Thus the study of the present circuit has considerable relevance in understanding SNA transitions.

In the present proposed circuit with a square wave force as one of the quasiperiodic forces in addition to a sinusoidal force, we have identified a route for the formation of a SNA which we term the *bubbling route* to SNA. In this route,

*Present address: Interdisciplinary Centre for Dynamics of Complex Systems, University of Potsdam, Germany.
†lakshman@cnld.bdu.ac.in

TABLE I. Routes and mechanisms for the formation of SNAs.

Type of route	Mechanism
Heagy-Hammel [16]	Collision of period-doubled torus with its unstable parent
Gradual fractilization [13]	Increased wrinkling of torus without any interaction with nearby periodic orbits
Type-I intermittency [10]	Due to saddle-node bifurcation, a torus is replaced by SNA
Type-III intermittency [22]	Subharmonic instability
Crisis-induced intermittency [14]	Doubling of destroyed torus involves a sudden widening of the attractor
Homoclinic collision [17]	Homoclinic collisions of the quasiperiodic orbits
Blowout bifurcation [6]	Due to changes in sign of the Lyapunov exponent Λ_T transverse to the invariant subspace S
Quasiperiodic route [9,11]	Collision between a stable and an unstable torus

bubbles appear in the strands of the torus as a function of the control parameter, then the sizes of the bubbles increase with the value of the control parameter, and subsequently strands of the bubbles become increasingly wrinkled, resulting in the creation of a SNA (while the remaining parts of the strands of the torus outside the bubbles remain largely unaffected). The mechanism for this route is that the quasiperiodic orbit becomes increasingly unstable in its transverse direction as a function of the control parameter, which is induced by the square-wave-type quasiperiodic force resulting in an increase in the size of the doubled strands (bubbles) in certain parts of the main strand and then the doubled strands become extremely wrinkled (without a complete doubling of the entire main strand), resulting in the SNA. In addition to this, we have also observed four other prominent routes in the same circuit, which include the fractalization, fractalization followed by intermittency, intermittency, and Heagy-Hammel routes, the details of which will be presented elsewhere.

In order to confirm the existence of the bubbling route to the SNA in the proposed circuit, we first present a detailed numerical analysis of the dynamical equations of the circuit in a rescaled form for suitable values of the parameters, using various qualitative and quantitative measures to establish this route. These include the Poincaré surface of section, the Fourier spectrum, the largest Lyapunov exponent and its variance, the spectral distribution function, and the distribution of finite-time Lyapunov exponents. A short account of these measures is given in the Appendix. Next, we confirm the results experimentally using the phase portraits of the quasiperiodic attractors and SNAs for the corresponding values of the circuit parameters, again with appropriate quantification measures, to establish the existence of a torus and the creation of a SNA through the bubbling route.

The paper is organized as follows. In Sec. II, we discuss the circuit realization of the quasiperiodically forced negative conductance series *LCR* circuit with a diode using a sinusoidal and a nonsinusoidal (square wave) forcing as quasiperiodic forces. In Sec. III, we describe the phase diagram of the circuit where the regions corresponding to the different dynamical transitions to SNAs are delineated as a function of the control parameters, based on our numerical analysis. The creation of the SNA via the bubbling route as confirmed in the numerical analysis is discussed in Sec. IV. Experimental confirmation of the bubbling route to the SNA is presented in Sec. V. Finally, we summarize our results in Sec. VI. The Appendix contains a short summary on the identification and characterization of SNAs and the associated routes.

II. CIRCUIT REALIZATION

In this section details about the proposed circuit are presented and the circuit equations are written in terms of the circuit variables. Then the circuit equations are transformed into dimensionless equations (normalized equations) using appropriate rescaled variables, for a convenient numerical analysis.

A. Experimental realization: Circuit equations

We consider the simple second-order nonlinear dissipative nonautonomous negative conductance series *LCR* circuit with a sinusoidal voltage generator $f_1(t)$ introduced by us recently [24,37], along with a second nonsinusoidal force $f_2(t)$, as shown in Fig. 1(a). The circuit consists of a series *LCR* network, forced by a sinusoidal voltage generator $f_1(t)$ and a nonsinusoidal (square wave) voltage generator $f_2(t)$ (HP 33120A series). Two extra components, namely, a *p-n* junction diode (D) and a linear negative conductor g_N, are connected in parallel to the forced series *LCR* circuit. The negative conductor used here is a standard op-amp based negative impedance converter. The diode operates as a nonlinear conductance, limiting the amplitude of the oscillator. In Fig. 1(a), v, i_L, and i_D denote the voltage across the capacitor C, the current through the inductor L, and the current through the diode D, respectively. The actual v-i characteristic of the diode [Fig. 1(b)] is approximated by the usual two-segment piecewise-linear function [Fig. 1(c)] which facilitates numerical analysis considerably. The state equations governing the presently proposed circuit (Fig. 1) are a set of

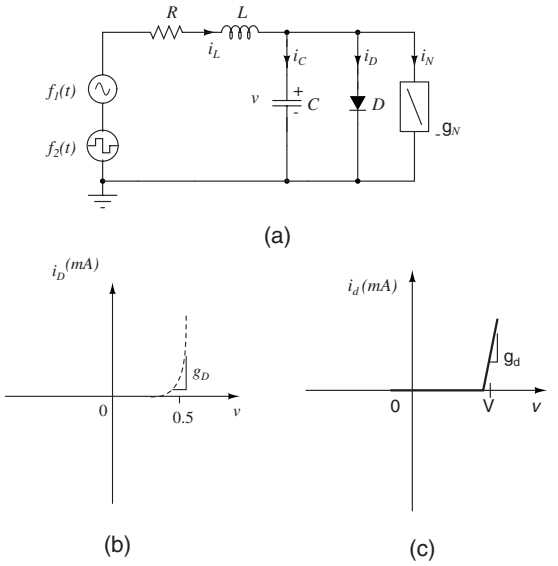

FIG. 1. (a) Circuit realization of a simple nonautonomous circuit. Here D is the p-n junction diode and g_N is negative conductance. The external emfs are $f_1(t)=E_{f1}\sin(\omega_{f1}t)$ and $f_2(t)=E_{f2}\,\mathrm{sgn}[\sin(\omega_{f2}t)]$. The values of the circuit elements are fixed as $L=50.3$ mH, $C=10.35$ nF, $R=1900\ \Omega$, $E_{f2}=400$ mV, and $\omega_{f2}=17\,033$ Hz. The forcing amplitude E_{f1} and its frequency ω_{f1} are chosen as the control parameters. (b) i-v characteristics of the p-n junction diode. (c) Two-segment piecewise-linear function.

two first-order nonautonomous differential equations

$$C\frac{dv}{dt}=i_L-i_D+g_Nv, \tag{1a}$$

$$L\frac{di_L}{dt}=-Ri_L-v+E_{f1}\sin(\omega_{f1}t)+E_{f2}\,\mathrm{sgn}[\sin(\omega_{f2}t)], \tag{1b}$$

where

$$i_D(v)=\begin{cases} g_D(v-V), & v\geqslant V,\\ 0, & v<V.\end{cases} \tag{1c}$$

Here g_D is the slope of the characteristic curve of the diode, E_{f1} and E_{f2} are the amplitudes, ω_{f1} and ω_{f2} are the angular frequencies of the forcing functions $f_1(t)=E_{f1}\sin(\omega_{f1}t)$ and $f_2(t)=E_{f2}\,\mathrm{sgn}[\sin(\omega_{f2}t)]$, respectively. In the absence of $f_2(t)$, the circuit [Fig. 1(a)] has been shown to exhibit chaos and also strong chaos not only through the familiar period-doubling route but also via torus breakdown followed by period-doubling bifurcations [37]. Here our aim is to investigate the effect of the second square wave type external forcing on the dynamics and to identify different types of transitions to SNAs.

In order to select the appropriate set of experimental parameters for which SNAs can be actually observed, we first carry out a detailed numerical simulation (as pointed out below) which then serves as a guide and a characterizer for experimental investigation. Using such an analysis, the values of the diode conductance g_D, negative conductance g_N, and break voltage V are fixed as 1313 μS, −0.45 mS, and 0.5 V, respectively. We have fixed the actual experimental values of the resistance R, inductance L, capacitance C, external frequency ω_{f2}, and forcing strength E_{f2} of the square wave as 1900 Ω, 50.3 mH, 10.35 nF, 17 033 Hz, and 400 mV, respectively, while we vary the amplitude E_{f1} and the frequency ω_{f1} of the sinusoidal force as control parameters in order to observe the various dynamical states. The forcing functions $f_1(t)$ and $f_2(t)$ are obtained from two separate function generators of the type HP 33120A.

B. Numerical analysis: Normalized equations

In order to study the dynamics of the circuit in detail, Eqs. (1a)–(1c) can be converted into a convenient normalized form for numerical analysis by using the following rescaled variables and parameters: $\tau=t/\sqrt{LC}$, $x=v/V$, $y=(i_L/V)(\sqrt{L/C})$, $E_1=E_{f1}/V$, $E_2=E_{f2}/V$, $\omega_1=\omega_{f1}\sqrt{LC}$, $\omega_2=\omega_{f2}\sqrt{LC}$, $a=R\sqrt{C/L}$, $b=g_N\sqrt{L/C}$, and $c=g_D\sqrt{L/C}$. The normalized evolution equation so obtained from Eq. (1a)–(1c) is

$$\dot{x}=y+f(x), \tag{2a}$$

$$\dot{y}=-x-ay+E_1\sin(\phi)+E_2\,\mathrm{sgn}[\sin(\theta)], \tag{2b}$$

$$\dot{\phi}=\omega_1, \tag{2c}$$

$$\dot{\theta}=\omega_2, \tag{2d}$$

where

$$f(x)=\begin{cases}(b-c)x+c, & x\geqslant 1,\\ bx, & x<1.\end{cases} \tag{2e}$$

Here the overdot stands for differentiation with respect to τ. Equation (2a)–(2e) is then numerically integrated using a Runge-Kutta fourth-order routine to identify the different dynamical scenarios corresponding to different values of the rescaled parameters. Various interesting dynamical transitions of Eq. (2a)–(2e) are described below.

III. TWO-PARAMETER PHASE DIAGRAM

The parameter space of the amplitude of the external forcing E_1 and the frequency ω_1 of the sinusoidal forcing is scanned first numerically in the range of $E_1\in(0.4,1.1)$ and $\omega_1\in(1.075,1.275)$ to pinpoint different dynamical behaviors and more specifically for the occurrence of SNAs through different routes. From this analysis, various dynamical transitions are determined as a function of the amplitude of the external forcing E_1 and its frequency ω_1. Further, these dynamical behaviors and their transitions are also confirmed experimentally for the corresponding values of the experimental parameters of the circuit given in Fig. 1.

A. Numerical analysis

To start with, we first demarcate the parameter space (E_1,ω_1), by numerically integrating Eqs. (2a)–(2e), into quasiperiodic, strange nonchaotic, and chaotic regimes by using the various qualitative and quantitative measures as dis-

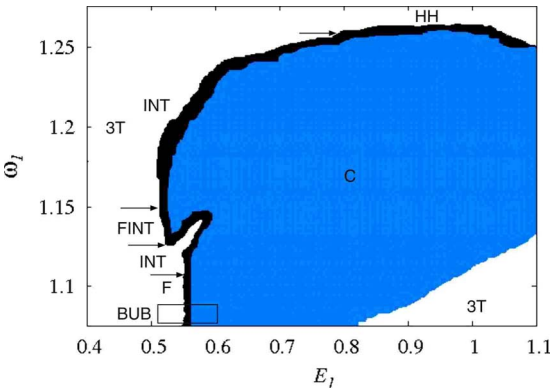

FIG. 2. (Color online) Numerical phase diagram in the $(E_1$-$\omega_1)$ plane for the circuit given in Fig. 1, represented by Eqs. (2a)–(2e). 3T correspond to period-3 torus, F, BUB, FINT, INT, and HH denote the creation of SNAs through the gradual fractalization, bubbling, fractalization followed by intermittency, intermittency, and Heagy-Hammel routes, respectively. C corresponds to the chaotic attractor. Arrows indicate the transition regions between two different types of route to the SNA.

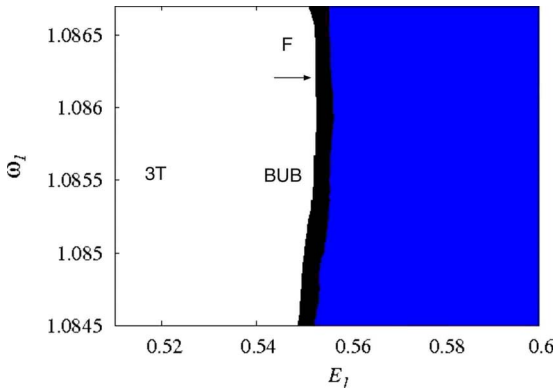

FIG. 3. (Color online) Blowup of Fig. 2 in the bubbling transition regime indicated as BUB.

cussed in the Appendix. The numerical phase diagram is shown in Fig. 2 for $E_1 \in (0.4, 1.1)$ and $\omega_1 \in (1.075, 1.275)$. The various dynamical behaviors indicated in the phase diagram (Fig. 2) and the interesting dynamical transitions are elucidated in the following.

Transitions from the quasiperiodic attractor to the SNA and subsequently to the chaotic attractor occur on increasing the value of the amplitude of the sinusoidal force E_1 for a fixed value of its frequency ω_1. Strange nonchaotic attractors created through different mechanisms are found to occur for different values of the frequency ω_1 of the sinusoidal force. Now, we will outline the ranges of values of the frequency ω_1 for which SNAs arise from quasiperiodic attractors through different mechanisms on increasing the value of the amplitude E_1 of the sinusoidal force.

A strange nonchaotic attractor created through the proposed route, namely, the bubbling route, is identified in the range of frequency $\omega_1 \in (1.085, 1.086)$. Here bubbles appear in the strands of period-3 torus and then the bubbles get increasingly wrinkled in the range of the amplitude $E_1 \in (0.54, 0.55)$ of the sinusiodal forcing resulting in the SNA. This phenomenon is named the bubbling transition to the SNA and it is denoted as BUB in Fig. 2. A blowup of the two-parameter space corresponding to the bubbling transition is shown in Fig. 3. A further increase in the value of E_1 ends up in the chaotic behavior indicated as C in Figs. 2 and 3. A strange nonchaotic attractor created through gradual fractalization (F) of the period-3 (3T) quasiperiodic attractor is identified for $\omega_1 \in (1.086, 1.111)$ as a function of the amplitude $E_1 \in (0.5, 0.55)$. The intermittency route (INT) is found to be exhibited in the range of frequency $\omega_1 \in (1.111, 1.1268)$ on increasing E_1 in the range $E_1 \in (0.5, 0.55)$ and also for $\omega_1 \in (1.1512, 1.2615)$ when $E_1 \in (0.5, 0.8)$. When the frequency $\omega_1 \in (1.1268, 1.1512)$, gradual fractalization is followed by intermittency phenomenon on increasing the value of the amplitude of the external forcing E_1. It is marked as (FINT) in Fig. 2. Torus-doubling bifurcation from a period-3 torus (3T) to a period-6 (6T) torus and then to a SNA via the Heagy-Hammel (HH) mechanism is found to occur in the range of $\omega_1 \in (1.2501, 1.2615)$ on decreasing E_1 in the range $E_1 \in (1.1, 0.8)$. The transition regions between the above-mentioned dynamical regimes are indicated by arrows in Fig. 2; they are fixed by scanning the frequency ω_1 of the sinusoidal force at its fourth decimal place. However, we do not draw a distinct boundary between any two scenarios because this requires a very detailed numerical analysis on a finer parameter scale.

B. Experimental investigation

It has additionally been confirmed that the above dynamical behaviors are also exhibited by the experimental circuit for the corresponding values of the circuit parameters E_{f1} $(=VE_1)$ and ω_{f1} $[=\omega_1/\sqrt{LC}]$ by examining the two-dimensional projections of the corresponding attractors obtained by measuring the voltage v across the capacitor C and the current i_L through the inductor L which are connected to the X and Y channels of an oscilloscope, respectively. Here V is the break voltage. Then, a live picture of the corresponding power spectrum obtained from a digital storage oscilloscope (HP 54600 series) of the projected attractor has also been used to distinguish the different attractors. In addition to this, the experimental data of the corresponding attractors recorded using a 16-bit data acquisition system [AD12-16U(PCI)EH] at the sampling rate of 200 kHz have been analyzed quantitatively using the different quantification measures, namely, the spectral distribution function and the distribution of finite time Lyapunov exponents. This information is then utilized (i) to pinpoint the different dynamical behaviors, (ii) to distinguish the SNAs created through different mechanisms, and (iii) also to compare them with the results of numerical simulation. In the following, we will describe only bubbling transition in detail by both numerical simulation and experimental realization, while the results of other known routes will be presented elsewhere.

IV. BUBBLING ROUTE TO SNA: NUMERICAL ANALYSIS

As noted above, in this route, the bubbles appear in the strands of the torus as the value of the amplitude E_1 of the

sinusoidal forcing is increased for a fixed value of its frequency ω_1. The sizes of the bubbles increase further on increasing the amplitude E_1 and the bubbles increasingly get wrinkled (while the remaining parts of the strands of the torus outside the bubbles remain largely unaffected) resulting in the creation of a SNA. This bubbling route is observed in the rather narrow range of frequency $\omega_1 \in (1.085, 1.086)$ as a function of the amplitude of the sinusoidal forcing $E_1 \in (0.5, 0.55)$ indicated as BUB in Figs. 2 and 3. It is to be noted that this route is significantly different from the well-known fractalization route [13], where the entire strands of the n-period torus continuously deform and get extremely wrinkled as a function of the control parameter. The formation of SNAs through this bubbling route has been identified in the literature for the first time to the best of our knowledge. We have used both qualitative and quantitative measures, which are indicated in the Appendix, to confirm the route. The qualitative proof is given through the Poincaré surface of section by distinguishing geometrically between quasiperiodic attractors and SNAs. The quantitative confirmation is provided using three different measures. (i) The largest Lyapunov exponent and its variance are used to distinguish between the torus and the SNA, and SNA and chaotic attractors. (ii) Scaling laws deduced from the distribution function for quasiperiodic attractors and SNAs are used to distinguish them. (iii) Finally, different routes to SNAs are also distinguished by the different distributions of local Lyapunov exponents. More information on the characterization is given in the Appendix. In the following we provide details of the confirmation of the bubbling route.

A. Poincaré surface of section plots and power spectra

We have fixed the value of the frequency of the sinusoidal forcing as $\omega_1 = 1.0852$ for illustration and varied its amplitude in the range $E_1 \in (0.5, 0.55)$ to elucidate the emergence of bubbling route to SNA in the present system (2a)–(2e). The Poincaré surface of section plot of the three strands corresponding to period-3 torus for the value of $E_1 = 0.5$ is shown in Figs. 4(a) and 5(a). The corresponding phase portrait and power spectrum are depicted in Figs. 6(a)(i) and 6(a)(ii), respectively. As the value of the amplitude E_1 is increased further, bubbles start to appear in all the three strands starting from $E_1 = 0.516$. These are shown in Figs. 4(b) and 5(b) for $E_1 = 0.52$ and the corresponding phase portrait and power spectrum are shown in Figs. 6(b)(i) and 6(b)(ii), respectively. Further increase in the value of E_1 results in an increase in the size of the bubbles as shown in Figs. 4(c) and 5(c) for the value of $E_1 = 0.54$, whose phase portrait and power spectrum are shown in Figs. 6(c)(i) and 6(c)(ii), respectively. Beyond the value of $E_1 = 0.54$, the strands of bubbles deform and get increasingly wrinkled [while the other parts of the strands of period-3 torus outside the bubbles remain unaltered as seen in Fig. 5(d)] leading to the formation of the SNA as depicted in Fig. 4(d) for the value of $E_1 = 0.546$. The phase portrait and power spectrum for this value of E_1 are shown in Figs. 6(d)(i) and 6(d)(ii), respectively. Finally, to confirm that the SNA transits to a chaotic attractor beyond $E_1 = 0.55$, we have depicted the

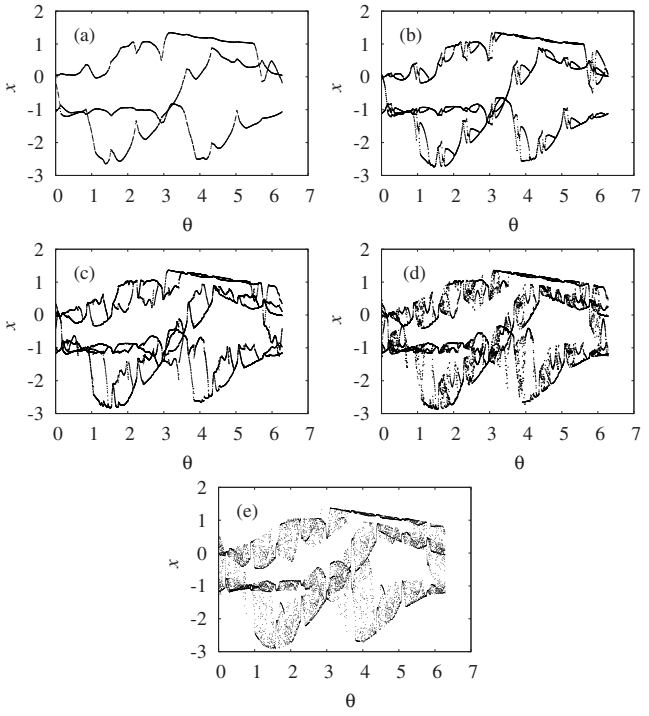

FIG. 4. Projection of the numerically simulated Poincaré surface of section of the attractors of Eqs. (2a)–(2e) in the (ϕ-x) plane for a fixed value of the frequency of the sinusoidal forcing, $\omega_1 = 1.0852$, as a function of its amplitude E_1, indicating the transition from a quasiperiodic attractor to a SNA through the bubbling route: (a) period-3 torus (3T) for $E_1 = 0.5$, (b) bubbled strands of period-3 torus (3T) for $E_1 = 0.52$, (c) enlarged bubbles in the strands of period-3 torus (3T) for $E_1 = 0.54$, (d) fractalized bubbles for $E_1 = 0.546$ with the remaining parts (away from the bubble) of the strands unaffected, and (e) chaotic attractor (widely interspersed bubbles) for $E_1 = 0.56$.

Poincaré surface of section of the latter in Figs. 4(e) and 5(e) with the corresponding attractor and power spectrum in Fig. 6(e) for $E_1 = 0.56$.

The mechanism for the bubbling route is that the quasiperiodic orbit becomes increasingly unstable in its transverse direction as a function of the control parameter (E_1), resulting in the formation of the doubled strands (bubbles), as seen in Figs. 4(b) and 5(b), in certain parts of the main strands. This instability of the quasiperiodic attractor arises due to the presence of the square wave pulse (finite amplitude for finite durations). Further increase in the value of the amplitude of the forcing (E_1) results in an increase in the size of the doubled strands (bubbles) as shown in Figs. 4(c) and 5(c), and then the doubled strands become extremely wrinkled (without a complete doubling of the entire main strand) resulting in the SNA as depicted in Figs. 4(d) and 5(d).

We now provide quantitative confirmation of the above results to distinguish between torus and SNA, and SNA and chaos.

B. Largest Lyapunov exponent and its variance

The largest Lyapunov exponent Λ and its variance μ, that is, the variance of Λ from finite-time Lyapunov exponents $\lambda_i(N)$, $i = 1, 2, \ldots, M$, of length N, defined as

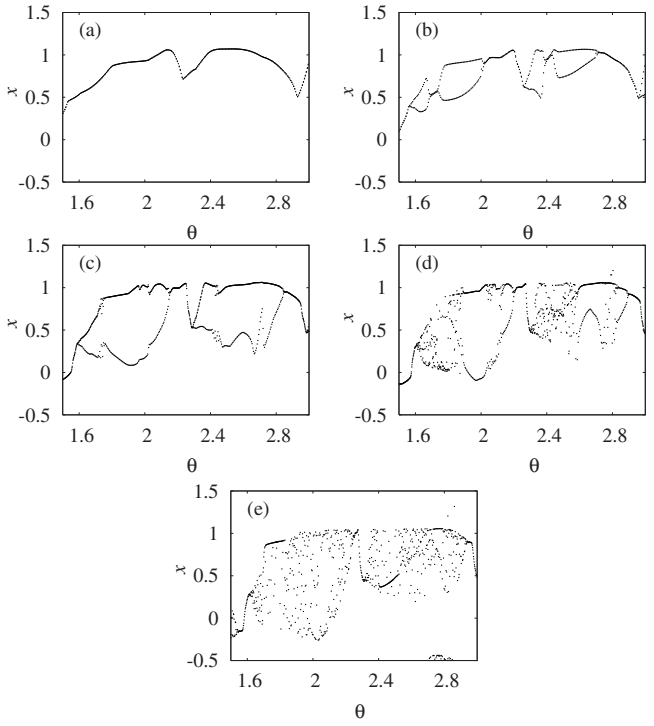

FIG. 5. Enlargments of Figs. 4 to show the bubbling transition to a strange nonchaotic attractor.

$$\mu = \frac{1}{M}\sum_{i=1}^{M}[\Lambda - \lambda_i(N)]^2 \tag{3}$$

are shown in Fig. 7 in the range of $E_1 \in (0.54, 0.546)$. The attractor depicted in Fig. 6(d)(i) for the value of $E_1 = 0.546$ is strange but it is nonchaotic as evidenced by the negative value of the Lyapunov exponent shown in Fig. 7(a). It is also to be noted that both the Lyapunov exponents and its variance [Fig. 7(b)] clearly indicate a critical value of amplitude $E_1^c = 0.5432$ ($E_1 < E_1^c$), below which a torus exists and above which ($E_1 > E_1^c$) the SNA appears. The regions of torus and SNA are clearly indicated by smooth and irregular variations, respectively, in the values of both the Lyapunov exponents Λ and its variance μ. Finally the transition of the SNA into a chaotic attractor is confirmed by the change in the largest Lyapunov exponent from negative to positive values at $E_1^c = 0.55$ as shown in the inset of Fig. 7(a).

C. Spectral distribution function and scaling laws

In order to distinguish further whether the attractors depicted in Figs. 6 are quasiperiodic or strange nonchaotic or chaotic attractors, we proceed to quantify the changes in their power spectra. The spectral distribution function, defined as the number of peaks in the Fourier amplitude spectrum larger than some value σ, is used to distinguish between quasiperiodic attractors and SNAs as well as SNAs and chaotic attractors. The quasiperiodic attractors obey a scaling relationship $N(\sigma) \sim \log_{10}(1/\sigma)$, while the SNAs satisfy a scaling power-law relationship $N(\sigma) \sim \sigma^{-\beta}, 1 < \beta < 2$ [2]. Similarly for the chaotic attractor, the scaling relation is $N(\sigma) \sim \sigma^{-\beta}, \beta > 2$.

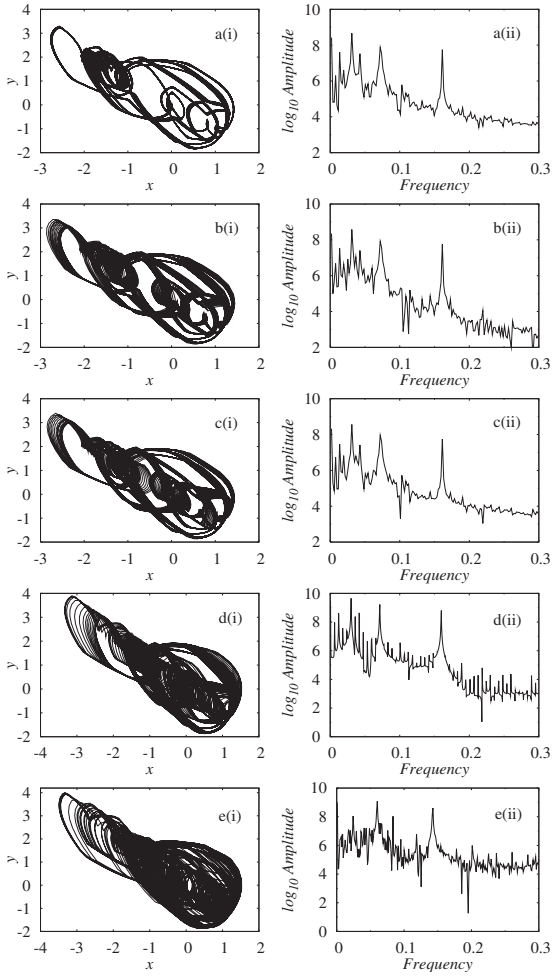

FIG. 6. Projection of the numerically simulated attractors and their power spectrum of Eqs. (2a)–(2e) for the same values of the frequency ω_1 and the amplitude E_1 of the sinusoidal forcing as in Figs. 4. (a) Period-3 torus (3T), (b) bubbled period-3 torus, (c) period-3 torus with enlarged bubbles, (d) fractalized bubbles (SNA), and (e) chaotic attractor: (i) phase portrait in the (x, y) space; (ii) power spectrum.

Spectral distribution functions (filled circles) of the torus [Fig. 6(a)] and bubbled torus [Fig. 6(b)] satisfy the scaling relation $N(\sigma) \sim \log_{10}(1/\sigma)$ as indicated by the solid line in Figs. 8(a) and 8(b), respectively, which is the characteristic of a torus. On the other hand the spectral distribution function of the SNA [Fig. 6(d)] exhibits power-law behavior as depicted in Fig. 8(c) (filled circles) with the value of the exponent $\beta = 1.88$, confirming the existence of the SNA. For the chaotic attractor [Fig. 6(e)], the scaling exponent [Fig. 8(d)] turns out to be $\beta = 3.5$ as required. Again the solid lines in Figs. 8(c) and 8(d) represent the scaling laws for SNA and chaos, respectively.

D. Distribution of local Lyapunov exponents

In addition to the qualitative discussion through the Poincaré surface of section plots in the (ϕ, x) plane (Figs. 4 and 5) in distinguishing the type of route through which the SNA appears, it is also possible to distinguish the route using

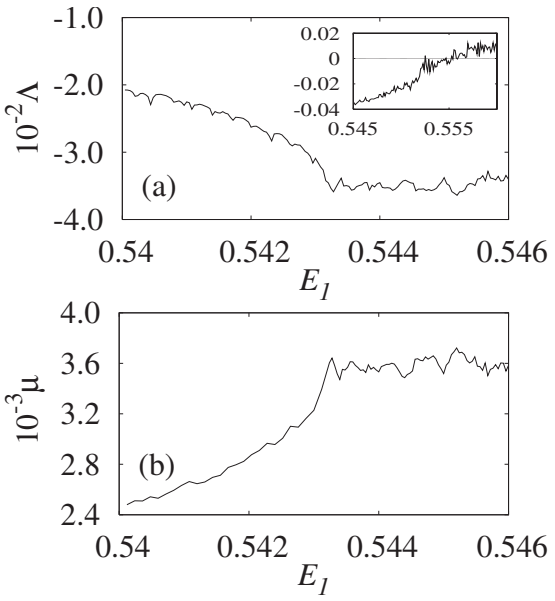

FIG. 7. Transition from torus to SNA through bubbling route for the same value of frequency as in Figs. 4 and in the range of amplitude $E_1 \in (0.54, 0.546)$ obtained numerically. (a) Largest Lyapunov exponent (Λ) and (b) its variance (μ). Inset in (a) depicts transition from SNA to chaos for $E_1 \in (0.545, 0.56)$.

the distribution of a quantitative measure, namely, finite-time Lyapunov exponents. It has been shown [10] that a typical trajectory on a SNA actually possesses positive Lyapunov exponents in finite time intervals, although the asymptotic exponent is negative. As a consequence, it is possible to observe different characteristics of SNAs created through different mechanisms by a study of the differences in the distribution of finite-time exponents $P(N,\lambda)$ [10]. The distribution can be obtained by taking a long trajectory and dividing it into segments of length N, from which the local Lyapunov exponent can be calculated. In the limit of large N, this distribution will collapse to a δ function $P(N,\lambda) \rightarrow \delta(\Lambda-\lambda)$. The deviations from—and the approach to—the

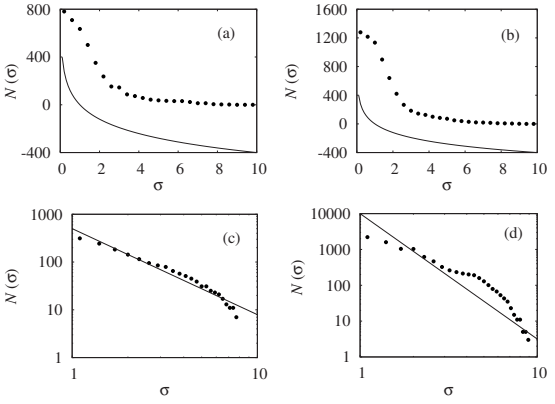

FIG. 8. Spectral distribution function (filled circles) calculated numerically. (a) Torus [Fig. 6(a)], (b) bubbled torus [Fig. 6(b)], (c) SNA [Fig. 6(d)], and (d) chaotic attractor [Fig. 6(e)]. Solid lines in (a) and (b) correspond to the scaling relation $N(\sigma) \sim \log_{10}(1/\sigma)$ and in (c) and (d) to the scaling relation $N(\sigma) \sim \sigma^{-\beta}$, with $\beta = 1.88$ and 3.5, respectively.

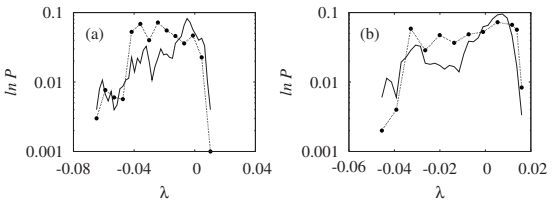

FIG. 9. Distribution of finite-time Lyapunov exponent calculated from both numerical data (solid line) and experimental data (dashed line) of (a) torus [Fig. 6(a)] and (b) SNA [Fig. 6(d)].

limit can be very different for SNAs created through different mechanisms [10].

We have calculated the distribution of local Lyapunov exponents $P(N,\lambda)$, for $N=2000$, for the attractors shown in Figs. 6(a)(i) and 6(d)(i) in order to confirm the nature of the transition to the SNA. The distribution of the local Lyapunov exponents for the period-3 torus (solid line) is shown in Fig. 9(a) in which the local Lyapunov exponents are peaked about the largest Lyapunov exponents (negative values) of the torus while that of the SNA shown in Fig. 9(b) by solid line has its maximum at a positive value of the local Lyapunov exponents. The distribution of local Lyapunov exponents for a SNA exhibits an elongated tail in its negative values because of the fact that in the bubbling transition parts of the strands of the period-3 torus remain unaffected even after the creation of the SNA, which contributes largely to the negative values. This confirms the existence of bubbling transition to strange nonchaotic attractors.

V. BUBBLING ROUTE TO THE SNA: EXPERIMENTAL CONFIRMATION

As a next step, in order to confirm the results of our numerical simulation in the experimental circuit shown in Fig. 1, a snapshot of the dynamical behavior for the corresponding values of the experimental parameters is obtained (as mentioned in Sec. II) and compared with that of the numerical results. Further, the corresponding experimental data are analyzed using various quantification measures mentioned in the previous section to confirm the nature of the dynamical behavior.

A. Phase portraits and power spectra

We have depicted the snapshots of the phase portraits and the corresponding power spectra of the attractors as seen in the oscilloscope (which is connected to the circuit shown in Fig. 1) in Fig. 10 for the corresponding values of the parameters of numerical simulation. The experimental period-3 torus and its power spectrum corresponding to the numerical results, Fig. 6(a), are shown in Figs. 10(a)(i) and 10(a)(ii). The attractors in the bubbling regime for the values of the amplitude of the sinusoidal forcing $E_{f1}=0.26$ and 0.27 V are shown in Figs. 10(b)(i) and 10(c)(i), respectively. The corresponding power spectra are shown in Figs. 10(b)(ii) and 10(c)(ii), respectively. The experimental phase portrait of the strange nonchaotic attractor and its power spectrum for the value of $E_{f1}=0.273$ V are depicted in Figs. 10(d)(i) and

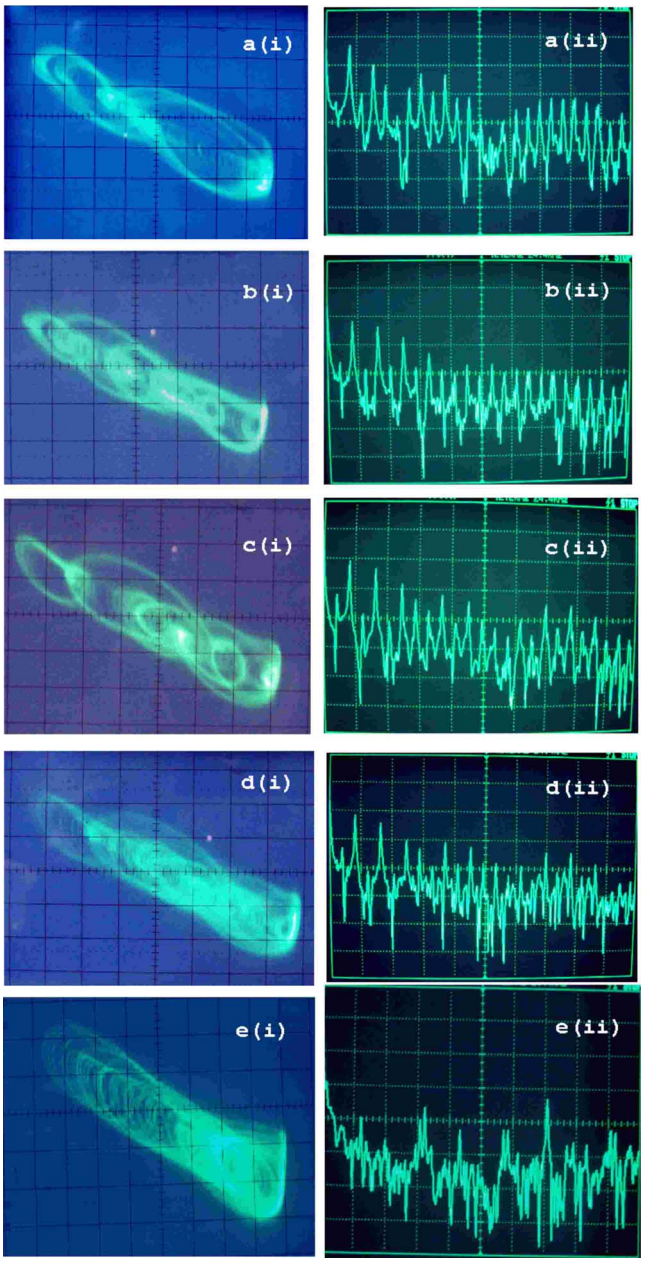

FIG. 10. (Color online) Snapshots of the experimental attractors and their power spectrum of the circuit shown in Fig. 1 for the corresponding values of the frequency ω_{f1} and the amplitude E_{f1} of the sinusoidal forcing in Fig. 4. (a) Period-3 torus (3T), (b) bubbled period-3 torus, (c) period-3 torus with enlarged bubbles, (d) fractalized bubbles (SNA), and (e) chaotic attractor: (i) phase portrait in the (v_C, i_L) space; (ii) power spectrum.

10(d)(ii), respectively. It is also seen that the spectra of the quasiperiodic attractors are concentrated at a small discrete set of frequencies while the spectrum of the SNA has a much richer set of harmonics. Further, the resemblance of the attractors illustrated in Figs. 10(i) with that of the attractors in Figs. 6(i) confirms the existence of the bubbling transition to the SNA in this negative conductance series *LCR* circuit with a diode having both sinusoidal and nonsinusoidal forces as quasiperiodic forcings. Finally, the chaotic attractor for E_{f1} =0.28 V and its power spectrum are shown in Fig. 10(e).

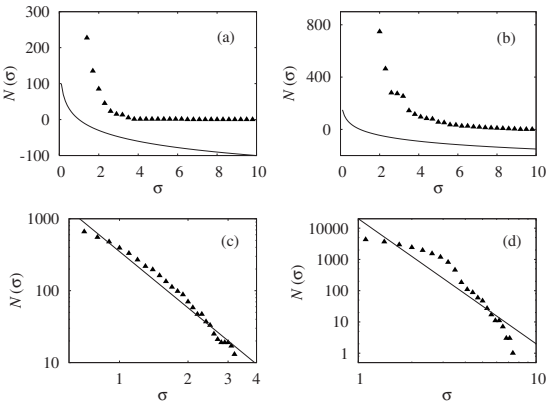

FIG. 11. Spectral distribution function (filled triangles) calculated from the experimental data of (a) torus [Fig. 10(a)], (b) bubbled torus [Fig. 10(b)], (c) SNA [Fig. 10(d)], and (d) chaotic attractor [Fig. 10(e)]. Solid curve and line in (a) and (b) correspond to the scaling relationship for the quasiperiodic attractors and in (c) and (d) to the scaling relation for the SNA and chaotic attractor, respectively.

B. Spectral distribution function and scaling laws

In order to confirm that the experimental phase portraits shown in Figs. 10(a), 10(b), 10(d), and 10(e) are indeed those of the torus, bubbled torus, SNA, and chaotic attractor, respectively, the corresponding data are examined for the behavior of their spectral distribution. Figures 11(a) and 11(b) show the spectral distribution function (filled triangles) for the torus in Figs. 10(a) and 10(b) satisfying the scaling relation $N(\sigma) \sim \log_{10}(1/\sigma)$ as indicated by the solid lines while that of the SNA [Fig. 10(d)] shown in Fig. 11(c) obey power-law distribution with the value of the exponent β =1.96 lying within the characteristic value for SNAs. For the chaotic attractor [Fig. 10(e)], the scaling exponent turns out to be β=4.0 [Fig. 11(d)] as expected.

C. Local Lyapunov exponents

Further, in order to examine whether the SNA shown in Fig. 10(d) arises from the bubbling transition, the distribution of the local Lyapunov exponents calculated from the experimental data of the torus [Fig. 10(a)] and the SNA [Fig. 10(d)] are depicted in Figs. 9(a) and 9(b), respectively, as dashed lines. The elongated tail in the distribution of the local Lyapunov exponents even for the SNA [Fig. 10(d)] confirms the existence of undisturbed strands as shown in Fig. 4(d), thereby confirming experimentally the creation of the SNA via the bubbling transition.

VI. SUMMARY AND CONCLUSION

In this paper, we have reported the creation of strange nonchaotic attractors through a route that we term the *bubbling route to a SNA* in a negative conductance series *LCR* circuit with a diode containing a nonsinusoidal (square wave) force as one of the quasiperiodic forcings. First, we presented the numerical analysis of the dynamical system, namely, Eq. (1a)–(1c) of the circuit (Fig. 1) for suitable

TABLE II. Different signatures of the largest Lyapunov exponents and its variance, and the distribution of finite-time Lyapunov exponents for the formation of three prominent types of SNAs.

Type of route	Lyapunov exponent Λ	Variance μ	Distribution of finite-time Lyapunov exponents $P(N,\lambda)$
Heagy-Hammel [16]	Irregular in the SNA region and smooth in the torus region	Small in torus and large in SNA	Distribution shifts continuously to larger exponents but the shape differs for torus and SNA
Gradual fractalization [13]	Increases slowly during the transition from torus to SNA	Increases only slowly	Distribution shifts continuously to larger exponents but the shape remains the same for torus and SNA
Intermittency [10,22]	Abrupt change during the transition from torus to SNA	Abrupt change at the transition point	Stretched exponential tail and asymmetric distribution

ranges of the amplitude E_1 and the frequency ω_1 of the sinusoidal force while the other parameters are held fixed. Following this, we have also confirmed the numerical results experimentally by the snapshots of the phase portraits of the quasiperiodic attractors and SNAs as well as chaotic attractors for the corresponding values of the circuit parameters. Further, the numerical and experimental data have been analyzed using various quantification measures, indicating the existence of torus, SNA, creation of SNA through the bubbling route, and transition to chaos. In particular, we have characterized the quasiperiodic attractors, SNAs and chaotic attractors using the maximal Lyapunov exponent and its variance, Poincaré maps, Fourier amplitude spectra, spectral distribution function, and distribution of finite-time Lyapunov exponents. The distribution of local Lyapunov exponents indeed clearly distinguishes the characteristic properties of both the torus and the SNA, confirming the existence of the bubbling route to the SNA. The experimental observations, numerical simulations, and characteristic analysis showed that the simple dissipative negative conductance series *LCR* circuit even with a nonsinusoidal (square wave) force as one of the quasiperiodic forces does indeed admit strange nonchaotic behaviors of different types and, in particular, admits a bubbling route to a SNA.

ACKNOWLEDGMENTS

This work has been supported by a Department of Science and Technology, Government of India sponsored IRHPA research project. The work of M.L. has been supported by DST Ramanna Program and D.V.S. has been supported by Alexander von Humboldt Foundation.

APPENDIX: IDENTIFICATION AND CHARACTERIZATION OF SNAs AND THEIR ROUTES

The torus, SNA, and chaotic attractors and the transitions between them through different routes can be identified and characterized through various qualitative and quantitative measures. In this appendix, we summarize the main measures used in the recent literature [8–10,14,18–24] in the analysis of transitions to SNAs from torus attractors and from SNAs to chaotic attractors. In the present work also we utilize these measures.

1. Qualitative measures

Geometrically smooth (torus) and nonsmooth (SNAs and chaotic) attractors can be distinguished qualitatively using the Poincaré surface of sections and Fourier spectra. The Poincaré surface of section shows smooth strands for quasiperiodic attractors, nonsmooth strands for SNAs, widely interspersed points throughout the phase space for chaotic attractors, which clearly reveals whether an attractor possesses a geometrically smooth or complicated structure. The spectra of the quasiperiodic attractors are concentrated at a small discrete set of frequencies while the spectra of SNAs and chaotic attractors have a much richer set of harmonics.

Further, different types of routes to SNAs and their mechanisms for their formation can also be identified qualitatively using the Poincaré surface of sections by observing the nature of the dynamics in these plots as a function of the control parameter. Different routes for the formation of SNAs have different characteristic dynamics in their Poincaré surface of section.

2. Quantative measures

(a) The largest Lyapunov exponents can be used to distinguish between (i) a torus and SNAs and (ii) SNAs and chaotic attractors. Torus motion is characterized by a smooth negative Lyapunov exponent, SNAs are characterized by either zero or nonsmooth negative Lyapunov exponents as a function of control parameters, and chaotic attractors have at least one positive Lyapunov exponent. Further, the transition from torus to SNAs exhibits different signatures in the values of the largest Lyapunov exponents and their variance for different routes to SNAs [14].

(b) Further, the torus and SNA can also be distinguished quantitatively by using the spectral distribution function, which is defined as the number of peaks in the Fourier amplitude spectrum larger than some value σ [3]. The quasiperiodic attractors obey a scaling relationship $N(\sigma) \sim \log_{10}(1/\sigma)$, while the SNAs satisfy a scaling power-law relationship $N(\sigma) \sim \sigma^{-\beta}, 1 < \beta < 2$. For chaos, the scaling exponent $\beta > 2$.

(c) A finer distinction between the different types of routes for the formation of SNAs can also made using the distribution of finite-time Lyapunov exponents. Different routes are characterized by different types of the distribution of finite-time Lyapunov exponents [10].

The different signatures of the above quantitative measures corresponding to different scenarios (routes) for the formation of three well-known types of SNAs are tabulated in Table II.

[1] C. Grebogi, E. Ott, S. Pelikan, and J. A. Yorke, Physica D **13**, 261 (1984).

[2] F. J. Romeiras and E. Ott, Phys. Rev. A **35**, 4404 (1987); F. J. Romeiras, A. Bondeson, E. Ott, T. M. Andonsen, Jr., and C. Grebogi, Physica D **26**, 277 (1987).

[3] A. Bondeson, E. Ott, and T. M. Antonsen, Jr., Phys. Rev. Lett. **55**, 2103 (1985); Y. C. Lai, Phys. Rev. E **53**, 57 (1996).

[4] M. Ding, C. Grebogi, and E. Ott, Phys. Rev. A **39**, 2593 (1989); M. Ding and J. A. Scott Relso, Int. J. Bifurcation Chaos Appl. Sci. Eng. **4**, 533 (1994).

[5] J. F. Heagy and W. L. Ditto, J. Nonlinear Sci. **1**, 423 (1991); J. I. Staglino, J. M. Wersinger, and E. E. Slaminka, Physica D **92**, 164 (1996).

[6] T. Yalcinkaya and Y. C. Lai, Phys. Rev. Lett. **77**, 5039 (1996).

[7] T. Kapitaniak and J. Wojewoda, *Attractors of Quasiperiodically Forced Systems* (World Scientific, Singapore, 1993).

[8] A. Venkatesan, M. Lakshmanan, A. Prasad, and R. Ramaswamy, Phys. Rev. E **61**, 3641 (2000).

[9] A. Venkatesan and M. Lakshmanan, Phys. Rev. E **55**, 5134 (1997); **58**, 3008 (1998).

[10] A. Prasad, V. Mehra, and R. Ramaswamy, Phys. Rev. Lett. **79**, 4127 (1997); Phys. Rev. E **57**, 1576 (1998).

[11] A. S. Pikovsky and U. Feudel, Chaos **5**, 253 (1995); U. Feudel, J. Kurths, and A. S. Pikovsky, Physica D **88**, 176 (1995); A. S. Pikovsky and U. Feudel, J. Phys. A **27**, 5209 (1994); S. P. Kuznetsov, A. S. Pikovsky, and U. Feudel, Phys. Rev. E **51**, R1629 (1995); A. Witt, U. Feudel, and A. S. Pikovsky, Physica D **109**, 180 (1997).

[12] V. S. Anishchenko, T. E. Vadivasova, and O. Sosnovtseva, Phys. Rev. E **53**, 4451 (1996); O. Sosnovtseva, U. Feudel, J. Kurths, and A. S. Pikovsky, Phys. Lett. A **218**, 225 (1996); S. Kuznetsov, U. Feudel, and A. Pikovsky, Phys. Rev. E **57**, 1585 (1998).

[13] K. Kaneko, Prog. Theor. Phys. **71**, 140 (1984); T. Nishikawa and K. Kaneko, Phys. Rev. E **54**, 6114 (1996).

[14] A. Venkatesan and M. Lakshmanan, Phys. Rev. E **63**, 026219 (2001).

[15] B. R. Hunt and E. Ott, Phys. Rev. Lett. **87**, 254101 (2001); J. W. Kim, S. Y. Kim, B. R. Hunt, and E. Ott, Phys. Rev. E **67**, 036211 (2003); S. Y. Kim, W. Lim, and E. Ott, *ibid.* **67**, 056203 (2003); W. Lim and S. Y. Kim, J. Korean Phys. Soc. **3**, 514 (2004).

[16] J. F. Heagy and S. M. Hammel, Physica D **70**, 140 (1994).

[17] A. Prasad, R. Ramaswamy, I. I. Satija, and N. Shah, Phys. Rev. Lett. **83**, 4530 (1999).

[18] C. S. Zhou and T. L. Chen, Europhys. Lett. **38**, 261 (1997); R. Ramaswamy, Phys. Rev. E **56**, 7294 (1997); R. Chacon and A. M. Gracia-Hoz, Europhys. Lett. **57**, 7 (2002).

[19] S. Y. Kim and W. Lim, J. Phys. A **37**, 6477 (2004).

[20] T. Kapitaniak and L. O. Chua, Int. J. Bifurcation Chaos Appl. Sci. Eng. **7**, 423 (1997).

[21] T. Yang and K. Bilimgut, Phys. Lett. A **236**, 494 (1997); Z. Liu and Z. Zhua, Int. J. Bifurcation Chaos Appl. Sci. Eng. **6**, 1383 (1996); Z. Zhua and Z. Liu, *ibid.* **7**, 227 (1997).

[22] A. Venkatesan, K. Murali, and M. Lakshmanan, Phys. Lett. A **259**, 246 (1999).

[23] W. L. Ditto, M. L. Spano, H. T. Savage, S. N. Rauseo, J. F. Heagy, and E. Ott, Phys. Rev. Lett. **65**, 533 (1990); T. Zhou, F. Moss, and A. Bulsara, Phys. Rev. A **45**, 5394 (1992); W. X. Ding, H. Deutsch, A. Dinklage, and C. Wilke, Phys. Rev. E **55**, 3769 (1997); J. A. Ketoja and I. Satija, Physica D **109**, 70 (1997).

[24] K. Thamilmaran, D. V. Senthilkumar, A. Venkatesan, and M. Lakshmanan, Phys. Rev. E **74**, 036205 (2006).

[25] A. Prasad, S. S. Negi, and R. Ramaswamy, Int. J. Bifurcation Chaos Appl. Sci. Eng. **11**, 291 (2001); A. Prasad, A. Nandi, and R. Ramaswamy, *ibid.* **17**, 3397 (2007).

[26] U. Feudel, S. Kuznetsov, and A. Pikovsky, *Strange Nonchaotic Attractors: Dynamics between Order and Chaos in Quasiperiodically Forced Systems* (World Scientific, Singapore, 2006).

[27] T. Zhou, F. Moss, and A. Bulsara, Phys. Rev. A **45**, 5394 (1992).

[28] W. X. Ding, H. Deutsch, A. Dinklage, and C. Wilke, Phys. Rev. E **55**, 3769 (1997).

[29] J. A. Ketoja and I. Satija, Physica D **109**, 70 (1997).

[30] G. Ruiz and P. Parmananda, Phys. Lett. A **367**, 478 (2007).

[31] S. Graziani, P. Silar, and M. J. Daboussi, BMC Evol. Biol. **2**, 18 (2004).

[32] D. Dubnau and R. Losick, Mol. Microbiol. **61**, 564 (2006).

[33] A. R. Bulsara, E. Jacobs, T. Zhou, F. Moss, and L. Kiss, J. Theor. Biol. **154**, 531 (1991); A. Longtin, A. Bulsara, D. Pierson, and F. Moss, Biol. Cybern. **70**, 569 (1994).

[34] V. Chinarov and M. Menzinger, BioSystems **55**, 137 (2000).

[35] Z. M. Ge and W. Y. Leu, Chaos, Solitons Fractals **20**, 502 (2004).

[36] G. D. VanWiggeren and R. Roy, Science **279**, 1198 (1998); Phys. Rev. Lett. **81**, 3547 (1998).

[37] K. Thamilmaran, D. V. Senthilkumar, M. Lakshmanan, and A. Ishaq Ahmed, Int. J. Bifurcation Chaos Appl. Sci. Eng. **15**, 2 (2005).